HIPPOCAMPUS 27:378–392 (2017)

Impairments in Spatial Representations and Rhythmic Coordination of Place Cells in the 3xTg Mouse Model of Alzheimer's Disease

Alexandra J. Mably [1,2]* Brian J. Gereke,[1,3] Dylan T. Jones,[1,2] and Laura Lee Colgin[1,2,3]*

ABSTRACT: Alzheimer's disease (AD) is an irreversible and highly progressive neurodegenerative disease. Clinically, patients with AD display impairments in episodic and spatial memory. However, the underlying neuronal dysfunctions that result in these impairments remain poorly understood. The hippocampus is crucial for spatial and episodic memory, and thus we tested the hypothesis that abnormal neuronal representations of space in the hippocampus contribute to memory deficits in AD. To test this hypothesis, we recorded spikes from place cells in hippocampal subfield CA1, together with corresponding rhythmic activity in local field potentials, in the 3xTg AD mouse model. We observed disturbances in place cell firing patterns, many of which were consistent with place cell disturbances reported in other rodent models of AD. We found place cell representations of space to be unstable in 3xTg mice compared to control mice. Furthermore, coordination of place cell firing by hippocampal rhythms was disrupted in 3xTg mice. Specifically, a smaller proportion of place cells from 3xTg mice were significantly phase-locked to theta and slow gamma rhythms, and the theta and slow gamma phases at which spikes occurred were also altered. Remarkably, these disturbances were observed at an age before detectable Aβ pathology had developed. Consistencies between these findings in 3xTg mice and previous findings from other AD models suggest that disturbances in place cell firing and hippocampal rhythms are related to AD rather than reflecting peculiarities inherent to a particular transgenic model. Thus, disturbed rhythmic organization of place cell activity may contribute to unstable spatial representations, and related spatial memory deficits, in AD.

KEY WORDS: hippocampus; gamma rhythms; theta rhythms; CA1; place fields

[1] **Center for Learning and Memory, The University of Texas at Austin, Austin, Texas 78712;** [2] **Department of Neuroscience, The University of Texas at Austin, Austin, Texas 78712;** [3] **Institute for Neuroscience, The University of Texas at Austin, Austin, Texas 78712**

Additional Supporting Information may be found in the online version of this article.

Grant sponsor: Esther A. and Joseph Klingenstein Fund; Grant sponsor: Alzheimer's Association; Grant number: NIRP-14-305205; Grant sponsor: NSF Graduate Research Fellowship; Grant number: DGE-1110007.

*Correspondence to: Alexandra J. Mably and Laura Lee Colgin, The Center for Learning and Memory, The University of Texas at Austin, 1 University Station Stop C7000, Austin, TX 78712, USA. E-mail: amably@austin.utexas.edu and colgin@mail.clm.utexas.edu

Accepted for publication 19 December 2016.
DOI 10.1002/hipo.22697
Published online 29 December 2016 in Wiley Online Library (wileyonlinelibrary.com).

INTRODUCTION

Alzheimer's disease (AD) is an irreversible, highly progressive neurodegenerative disease and the leading form of dementia (Ferri et al., 2005). Clinically, AD initially manifests as subtle but progressive impairments in episodic and spatial memory (Hodges, 2000; Albert, 2011; McKhann et al., 2011). Yet, it remains largely unknown how the proteins that comprise the hallmark pathologies in AD—amyloid β-protein (Aβ) and microtubule-associated protein tau—affect the network dynamics believed to underlie episodic and spatial memory.

The hippocampal formation is critical for the acquisition and retrieval of episodic and spatial memories (Squire et al., 2004). The role of the hippocampus in spatial memory was sparked by the discovery of "place cells," neurons in the hippocampus that exhibit receptive fields for particular locations in space known as "place fields" (O'Keefe and Dostrovsky, 1971; O'Keefe, 1976). Place cell spiking is modulated by theta and gamma oscillations, and such rhythmic co-ordination is thought to be important for temporally organizing spatial memories (O'Keefe and Recce, 1993; Skaggs et al., 1996; Csicsvari et al., 2003; Bieri et al., 2014; Zheng et al., 2016). Recent results have further suggested that temporal organization of place cell representations of space is differentially affected by distinct slow (~25–55 Hz) and fast (~65–100 Hz) gamma rhythms (Zheng et al., 2016).

Place cell abnormalities have been reported in several mouse models of AD (Cacucci et al., 2008; Cheng and Ji, 2013; Zhao et al., 2014; Cayzac et al., 2015; Booth et al., 2016). Moreover, disturbed theta and gamma oscillations in the hippocampus have been observed in transgenic and Aβ injection models of AD (Villette et al., 2010; Rubio et al., 2012; Cheng and Ji, 2013; Ittner et al., 2014; Schneider et al., 2014; Cayzac et al., 2015; Ciupek et al., 2015; Gillespie et al., 2016; Iaccarino et al., 2016). However, to our knowledge, no previous study has assessed rhythmic coordination of place cells by slow and fast gamma oscillations in an AD mouse model. Increasing evidence suggests that slow and fast gamma rhythms reflect distinct information processing states

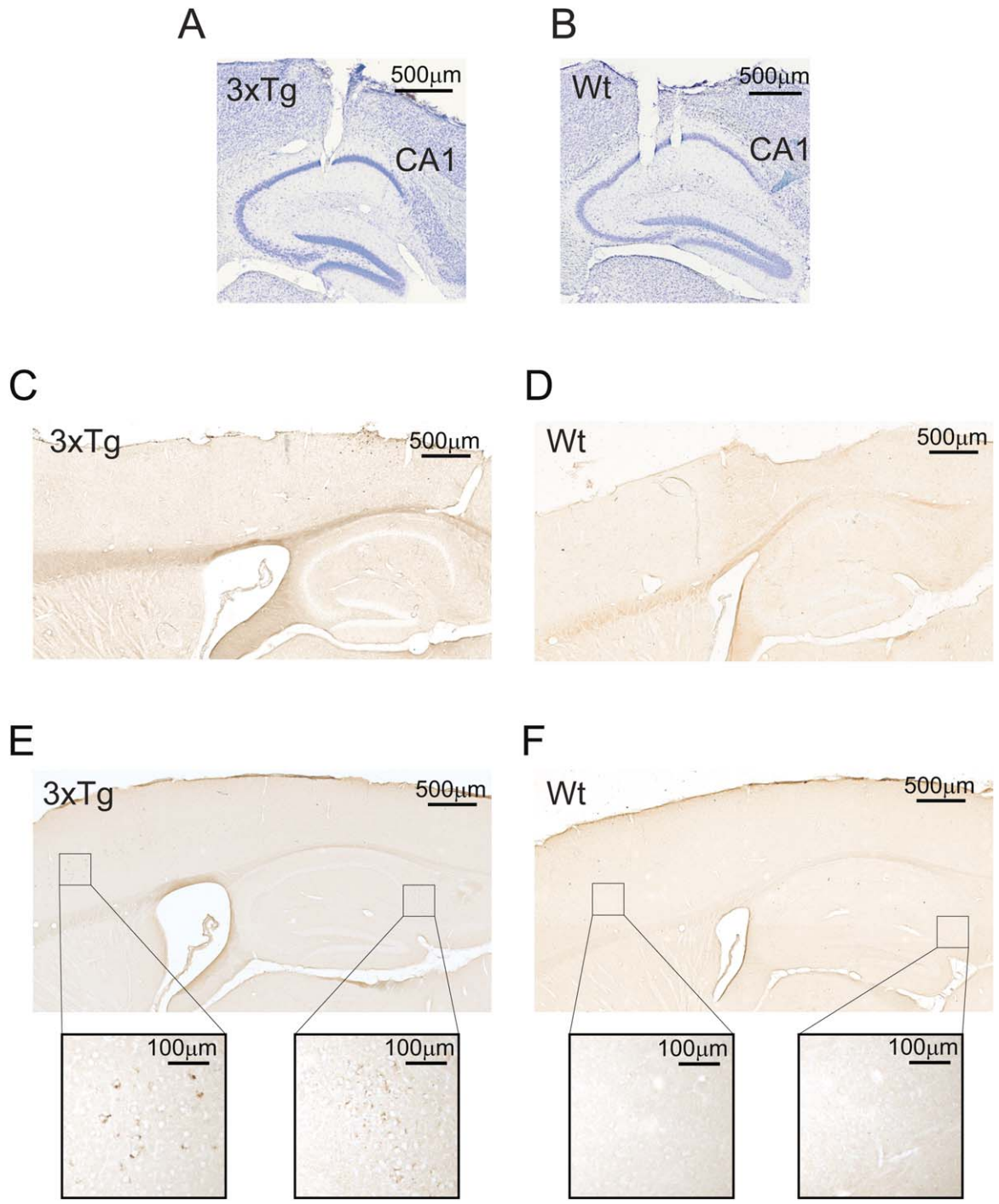

FIGURE 1. Verification of tetrode locations and investigation of Aβ pathology. (A,B) Cresyl violet stained sections from (A) 3xTg and (B) Wt mice confirming tetrode recording locations in CA1. (C,D) The anti-Aβ polyclonal antibody, DW6, was used to detect Aβ deposits in the 8–9-month-old (C) 3xTg and (D) Wt mice used for testing, revealing that the mice tested were in a pre-pathology disease stage. Intraneuronal Aβ deposits were confirmed in older (11–12 months old) (E) 3xTg mice, but not (F) Wt mice. (A–F) 5× magnification; selected areas of the neocortex and hippocampus are shown at 10× magnification (boxes in E,F).

in the hippocampal network (Colgin, 2015). Fast gamma rhythms in the hippocampus are coupled with fast gamma rhythms in the medial entorhinal cortex and thus may promote transmission of current sensory information to the hippocampus during new memory encoding (Colgin et al., 2009). Slow gamma rhythms link hippocampal subfield CA1 to inputs

from neighboring subfield CA3 (Colgin et al., 2009) and thus have been proposed to facilitate memory retrieval, considering that memories are thought to be stored in CA3 (Treves and Rolls, 1992; Nakazawa et al., 2002; Steffenach et al., 2002). Therefore, a failure in fast or slow gamma rhythmic co-ordination could produce deficits in memory encoding or memory retrieval, respectively. Remarkably, a recent study reported that AD mice correctly store, but cannot retrieve, memories (Roy et al., 2016). Taken together, these findings suggest that deficient slow gamma co-ordination of place cells may contribute to impairments in retrieval of stable representations of space in AD mice.

To test this hypothesis, we assessed firing properties and rhythmic coordination of place cells in the 3xTg mouse model. These mice are an AD model that harbors 3 disease-relevant mutations: human APP_{Swe}, $tau_{P301L,}$ and $presenilin\text{-}1_{PS1M146V}$ (Oddo et al., 2003a). Several disease-implicated Aβ species have been detected in the brains of 3xTg mice, including intraneuronal Aβ, oligomeric forms of Aβ, and amyloid deposits (Oddo et al., 2003a, 2003b, 2006). Furthermore, 3xTg mice exhibit spatial memory impairments (Billings et al., 2005). However, to our knowledge, no study has yet examined whether place cell representations of space and rhythmic coordination of place cell firing are impaired in 3xTg mice. Here, we recorded place cells and hippocampal rhythms in area CA1 of freely behaving 3xTg mice. We found that place cells in 3xTg mice exhibited reduced firing rates and spatial information. Additionally, place cell maps were significantly less stable in 3xTg mice than in wild type (Wt) mice. Furthermore, place cell spikes in 3xTg mice were significantly less phase-locked to theta and slow gamma rhythms than were spikes from Wt place cells. These results are consistent with the hypothesis that abnormal theta and slow gamma co-ordination of place cells contributes to deficient spatial memory retrieval in AD.

MATERIALS AND METHODS

Subjects

Animals for this study were kindly donated by the Zemelman Laboratory at The University of Texas at Austin (UT Austin). The Zemelman Laboratory obtained male and female B6;129-$Psen1^{tm1Mpm}$Tg (APP_{Swe}, tau_{P301L}) (3xTg) mice from Jackson Laboratories (Bar Harbor, ME). A 3xTg colony was then maintained at UT Austin by breeding homozygous pairs. Simultaneously, a B6;129 hybrid (Jackson Laboratories) colony of control mice was also maintained, hereafter referred to as wild type (Wt) mice. Mice were kept on a reverse light/dark cycle (lights off 9 am to 9 pm) and tested during the dark phase. Mice were group housed in a genotype-specific manner prior to surgery; mice were then individually housed following surgery. Three male 3xTg mice and three male Wt mice were used in this study. Physiological recordings were obtained from mice at 8–9 months of age. Mice recovered from recording drive implantation surgery (see "Implantation and tetrode placement" section below) for at least 1 week prior to the commencement of behavioral training and data acquisition. During the data collection period, mice were placed on a food-restricted regimen and maintained at ∼90% of their free-feeding body weight. An additional three naïve male 3xTg mice and one naïve male Wt mouse were sacrificed, and their brains were removed and processed for immunohistochemistry (see "Immunohistochemistry" section below). All experiments were conducted according to the guidelines of the NIH Guide for the Care and Use of Laboratory Animals under a protocol approved by the UT Austin Institutional Animal Care and Use Committee.

Recording Drive and Tetrode Preparation

Recording drives were custom-built using a modified version of a previously published design (Voigts et al., 2013). Drives contained 2 bundles spaced 4 mm apart. Each bundle contained 8 independently moveable tetrodes. Tetrodes were constructed from 17 μm polyimide-coated platinum–iridium (90–10%) wire (California Fine Wire). Electrode tips were plated with platinum to reduce single-channel impedances to ∼150–300 kΩ at 1 kHz.

Implantation and Tetrode Placement

Recording drives were surgically implanted with the 2 bundles targeting the bilateral hippocampi. Stereotaxic surgery coordinates were 2.0 mm AP, 2.0/−2.0 mm ML, and 0.5 mm DV. Six or seven bone screws were placed in the skull, and the two most anterior of these screws were connected to the recording drive ground. Dental cement was placed around the screws and the base of the drive to affix the drive securely to the skull. Tetrodes were slowly lowered to their target locations over the course of approximately 2 weeks following surgery. One tetrode from each bundle served as a reference for differential recording and was placed in a relatively quiet region at the level of the corpus callosum or higher. The remaining recording tetrodes were targeted toward the CA1 cell body layer. Tetrodes were turned at least 40 μm between recording days to prevent recordings of the same single units across multiple days. Different tetrodes reached the cell body layer at different depths and on different days, and thus place cell recordings were obtained from each mouse over the course of several (7–10) days. All recording locations were histologically verified following experiments; examples of recording locations are shown (Figs. 1A,B). Only single units recorded from tetrodes that were histologically verified to be in CA1 were used in this study. A total of 255 place cells from Wt mice and 198 place cells from 3xTg mice were recorded.

Testing Procedures

Following the postsurgery recovery period, mice were trained to run three 10-min sessions per day on a circular track 100 cm in diameter. The width of the track was 9 cm.

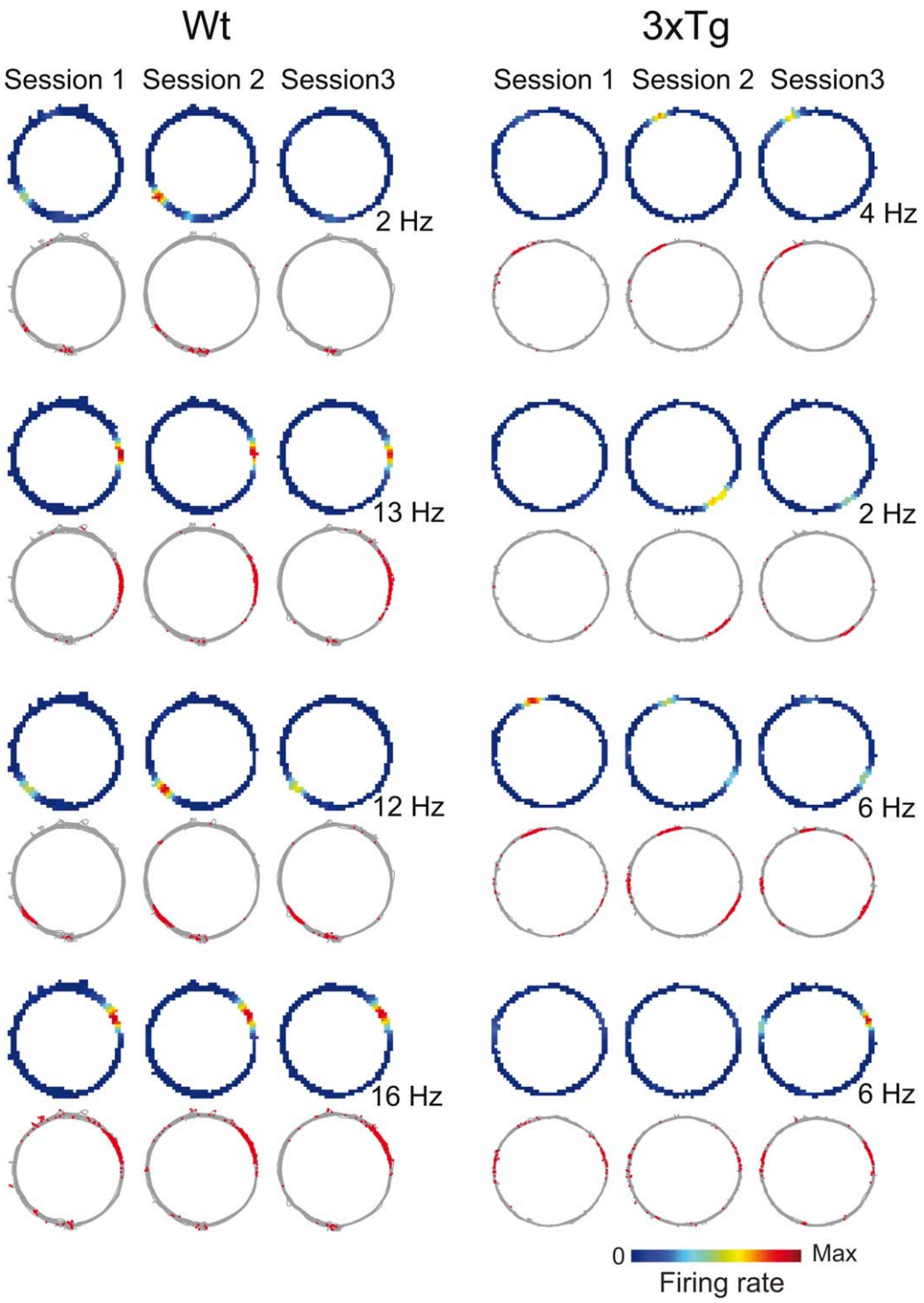

FIGURE 2. Place fields from 3xTg mice were less stable across time. Example place field maps from Wt (left panel) and 3xTg (right panel) mice running on a familiar circular track. Place field maps are shown for session 1 (left column), session 2 (middle column), and session 3 (right column). Color-coded rate maps were scaled to the peak firing rate across all three sessions (red indicates peak rate and dark blue indicates 0 Hz). For each map, the peak firing rate across the sessions is shown to the right. Paths traversed by the animal (grey lines) and corresponding spikes (red dots) are shown below each color-coded rate map. For each genotype, all place cells recorded from one example tetrode on one example day are shown.

Intersession intervals were 10 min, during which time the mice rested on a towel-covered pot in the recording room. Mice were trained to run unidirectionally around the track, receiving small pieces of cookie as a reward at one location on the track at the end of each circuit. The reward location remained constant within a day but was changed in a semi-random fashion

each day to prevent accumulation of place fields at particular reward sites (Hollup et al., 2001). To ensure that the environment was familiar, mice were trained on the circular track for at least 3 days prior to the start of recording.

Data Acquisition

Data were collected using a Neuralynx data acquisition system (Neuralynx, Bozeman, MT, USA). The recording drive was connected to two HS-36 headstages (Neuralynx). The headstage output was conducted via lightweight tether cables (TETH-HS-36-Litz, Neuralynx) through a multichannel slipring commutator to a data acquisition system that processed the signals through individual 24-bit analog to digital converters (Digital Lynx, Neuralynx). Unit activity was bandpass filtered from 600 to 6000 Hz. Spike waveforms with amplitudes that exceeded a threshold set by the experimenter ($\sim$50 μV) were time-stamped, and 1 ms windows centered around the spike peaks were recorded at a sampling rate of 32 kHz. Local field potentials (LFPs; 1 per tetrode) were recorded continuously in the 0.1–500 Hz band at a sampling rate of 2000 Hz. Notch filters were not used. Continuously sampled LFPs were recorded differentially against a common reference electrode (see "Implantation and tetrode placement" section above). Red and green light-emitting diodes on the headstages were used to track the animals' movements at a sampling rate of 30 Hz.

Spike Sorting and Cell Classification

Spike sorting was performed offline using graphical cluster cutting software (MClust; A. D. Redish, University of Minnesota, Minneapolis). Spikes were clustered manually in two-dimensional projections of the multidimensional parameter space (consisting of waveform amplitudes, energies, and peak-to-valley ratios). Additionally, autocorrelation functions were utilized to assist with identification of single units. Place cells were distinguished from putative interneurons on the basis of average firing rate, bursting properties, and spike width (Fox and Ranck, 1981; Harris et al., 2000; Henze et al., 2000). Cluster isolation statistics for single units from Wt and 3xTg mice were not significantly different (Supporting Information, Table S1).

Data Analysis and Statistics

Data are presented as mean $\pm$ SEM, unless otherwise indicated. Data were analyzed using custom software written in MATLAB (Mathworks). Statistics were computed with SPSS 23 (IBM) and Oriana 4 (Kovach Computing Services). Mann–Whitney *U* tests were used to compare lap-by-lap spatial correlations, lap-by-lap rate overlap scores, spatial information, firing rates, place field size, number of place fields per cell, cluster isolation measures, and running speeds. Rate overlap, spatial correlations, and mean vector lengths were compared using mixed model repeated measures ANOVAs. When Mauchly's assumption of sphericity was violated and ε was >0.75, the Huynh–Feldt correction (Huynh and Feldt, 1976) was applied (Girden, 1992). Binomial tests were used to compare the percentages of cells that were significantly phase-locked to LFP oscillations, with observations from Wt mice used as the expected proportion. Watson–Williams tests were used to compare preferred spike time phases.

Place Fields

For all place field analyses, spikes that occurred when running speeds were <3 cm/s were excluded to prevent inclusion of spikes from periods when mice paused to consume rewards. For Figures 2 and 3A–H, smoothed spatial firing rate distributions ("place maps") for each well-isolated place cell were constructed using a 4 cm SD Gaussian kernel evaluated on a square grid covering the environment with points spaced by 1.3 cm. Individual place fields were required to have at least 3 contiguous bins with firing rates above 1.5 Hz.

For measures of place field size, number of place fields per cell, and in-field firing rates (Figs. 3I,J and Supporting Information, Table S1), position estimates were linearized. Linearization was carried out by converting the Euclidean coordinates of the spikes to radians based on the known circumference of the circular track. The grid spacing for the linearized rate maps corresponded to 2.5 cm and a wrapped Gaussian kernel with an SD corresponding to 5 cm was used. The number of place fields for each place cell was calculated by first finding the peak firing rate bin in a set of contiguous bins with rates >1.5 Hz, then expanding in both directions and including all contiguous bins for which the firing rate was at least 10% of the peak firing rate. This process was then repeated until no further fields (i.e., at least 3 contiguous bins with peak rates above 1.5 Hz) were found in the rate map. Place field size was then estimated for each field by multiplying the bin size (i.e., 2.5 cm) with the number of bins in each field.

Spatial Correlation

Place fields across daily sessions were compared using a previously described spatial correlation method (Leutgeb et al., 2005; Colgin et al., 2010). The firing rates in pixels corresponding to the same spatial locations were correlated for each cell across sessions or laps (Figs. 3A,E).

Rate Overlap

A rate overlap measure was used that is similar to one described previously (Colgin et al., 2010). Specifically, the rate overlap between 2 sessions for each active cell was calculated by taking the ratio of the mean firing rate from each session's rate map, with the smaller of the two means as the numerator (Fig. 3B). Cells were considered active if they had peak and mean firing rates of >1.5 Hz and >0.5 Hz, respectively, in at least one session. Rate overlap between two laps (Fig. 3F) was calculated in the same manner except that the mean firing rate from each lap around the circular track was used rather than the mean firing rate within a session.

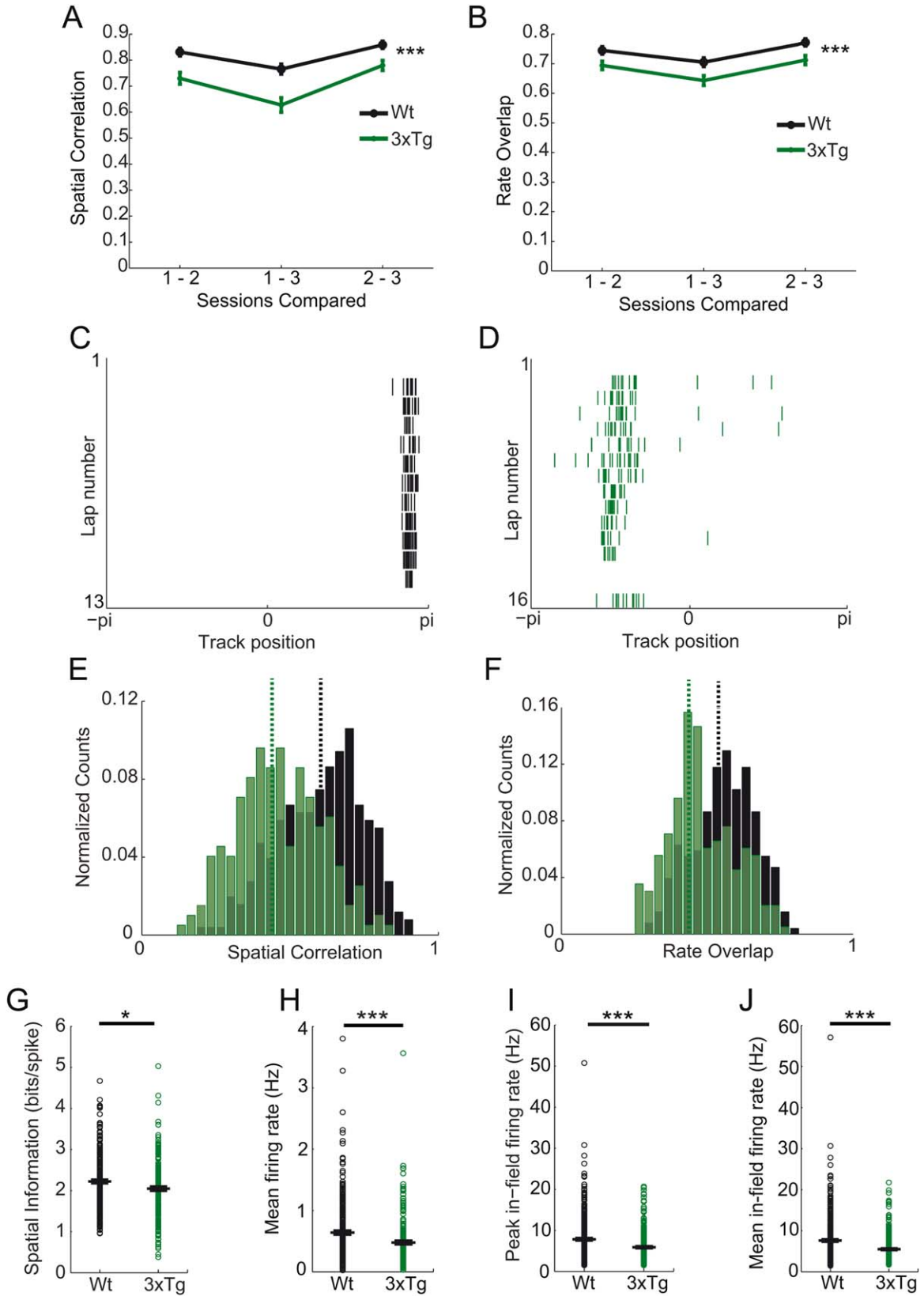
A
Spatial Correlation
0.9
0.8
0.7
0.6
0.5
0.4
0.3
0.2
0.1
0
***
Wt
3xTg
1 - 2
1 - 3
2 - 3
Sessions Compared
B
Rate Overlap
0.8
0.7
0.6
0.5
0.4
0.3
0.2
0.1
0
***
Wt
3xTg
1 - 2
1 - 3
2 - 3
Sessions Compared
C
Lap number
1
13
−pi
0
pi
Track position
D
Lap number
1
16
−pi
0
pi
Track position
E
Normalized Counts
0.12
0.08
0.04
0
0
Spatial Correlation
1
F
Normalized Counts
0.16
0.12
0.08
0.04
0
0
Rate Overlap
1
G
Spatial Information (bits/spike)
6
5
4
3
2
1
0
*
Wt
3xTg
H
Mean firing rate (Hz)
4
3
2
1
0
***
Wt
3xTg
I
Peak in−field firing rate (Hz)
60
50
40
30
20
10
0
***
Wt
3xTg
J
Mean in-field firing rate (Hz)
60
50
40
30
20
10
0
***
Wt
3xTg

FIGURE 3.

Spatial Information

Spatial information was calculated for each cell as previously described (Skaggs et al., 1996):

$$\text{Spatial information} = \sum_i P_i \frac{\lambda_i}{\lambda} \log 2 \frac{\lambda_i}{\lambda},$$

where i is an index over spatial bins, P_i is the probability of the animal being in the ith bin, λ_i is the mean firing rate in the ith bin, and λ is the overall mean firing rate of the cell (Fig. 3G).

Running Speed

The running speed (Supporting Information, Table S1) at each position (x_n) was estimated by taking the difference between the preceding position (x_{n-1}) and the following position (x_{n+1}) and dividing by the elapsed time.

Spike-Triggered Averages, Spike Time-Phase Estimates, and Percentage of Significantly Phase-Locked Cells

In our experience, tetrode recordings in mice may include some activity that is not locally generated (i.e., artifacts that are volume conducted across short distances in the small mouse brain). For this reason, we mainly focused our analyses on rhythmic modulation of spikes, under the assumption that rhythms that significantly modulate local spiking patterns are likely to be locally generated.

To calculate spike time-phase estimates, the time-varying phases of theta, slow gamma, and fast gamma were determined using the Hilbert transform of the bandpass filtered signal (Hamming window; 6–10 Hz passbands and 5–11 Hz stopbands for theta, 25–55 Hz passbands and 20–60 Hz stopbands for slow gamma, 65–100 Hz passbands and 60–105 Hz stopbands for fast gamma). The theta, slow gamma, and fast gamma spike time-phase distributions for each cell were then determined by identifying the theta, slow gamma, and fast gamma phases, respectively, at the EEG time point closest to each spike time. Phase-locking was quantified using the mean vector length of the resulting phase distributions (Fig. 4). For all CA1 place cells, spike time-phase estimates were obtained using the LFP from the tetrode on which the spike was recorded. The preferred firing phase for each single unit was defined as the mean of all spike time phases for each single unit. Place cells were considered to be significantly phase-locked to a particular oscillation if their spike phase distribution for that oscillation deviated significantly from uniformity ($P < 0.05$, Rayleigh test).

Spike-triggered averages (STAs) (Figs. 4C,F,I) were computed by averaging spike-centered segments of LFP recordings. To assess modulation of spikes by theta oscillations, 400 ms segments of unfiltered LFP were aligned according to spike times (i.e., 200 ms before and after each spike). To assess modulation of spikes by slow and fast gamma rhythms, 200 ms segments of slow gamma or fast gamma bandpass-filtered (as described above) LFP recordings were aligned with respect to spike times (i.e., 100 ms before and after each spike).

Time Frequency Representation of Gamma Power Across Theta Cycles

The time-varying power across frequencies (Fig. 5) was computed using a wavelet transform method as previously described (Tallon-Baudry et al., 1997; Colgin et al., 2009). Signals were convolved by a family of complex Morlet's wavelets $w(t,f)$, one for each frequency, as a function of time:

$$w(t,f) = A \exp\left(-\frac{t^2}{2\sigma_t^2}\right) \exp(2i\pi f t)$$

With $\sigma_f = 1/2\pi\sigma_t$. The coefficient A was set at

$$\left(\sigma_t \sqrt{\pi}\right)^{-1/2}$$

to normalize the wavelets such that their total energy was equal to 1. The family of wavelets was characterized by a constant ratio f/σ_f, which was set to 7.

Theta cycles were selected by bandpass filtering the signal from 4 to 12 Hz and selecting local minima in the filtered signal. Segments of the recording were then collected and defined as a theta cycle if the time between detected local minima corresponded to the period of an ~8 Hz theta cycle (i.e., 125 ± 25 ms). In addition, detected local minima were required to be separated by at least 100 ms. Time-varying

FIGURE 3. Irregular place cell firing properties in 3xTg mice. Data are shown for the entire population of place cells recorded from histologically verified recording sites in CA1. (A,B) Place cell maps in Wt mice were significantly more stable across the 3 daily sessions than place cell maps in 3xTg mice. (A) Spatial correlation and (B) rate overlap measures for 3xTg (green) and Wt (black) mice are shown. Asterisks indicate significant main effects of genotype. (A) Correlations between place cell maps on the circular track were calculated between all possible session pairs for the 3 daily sessions. (B) Same as A, but for the rate overlap measure. (C–F) Place cell maps in Wt mice were significantly more stable across laps within each session than place cell maps in 3xTg mice. Example spike raster plots for successive laps within a session for (C) a Wt and (D) a 3xTg place cell. Place cells from 3xTg mice had lower median (green dashed line for 3xTg and black dashed line for Wt) (E) spatial correlation and (F) rate overlap values than Wt place cells. (G) Place cells from Wt mice conveyed significantly more spatial information than place cells from 3xTg mice. (H–J) Place cells from Wt mice had significantly higher firing rates than place cells from 3xTg mice. Shown are (H) the mean firing rate across all locations, (I) the peak firing rate within the place field, and (J) the mean firing rate within the place field. Bars represent mean ± SEM in this and subsequent figures, unless indicated otherwise. (A,B; E,F; and G,H) Wt: $n = 255$ place cells; 3xTg: $n = 198$ place cells. (I,J) Wt: $n = 364$ place fields; 3xTg: $n = 274$ place fields. * indicates $p \leq 0.05$ and * indicates $p \leq 0.001$ in this figure and subsequent figures.**

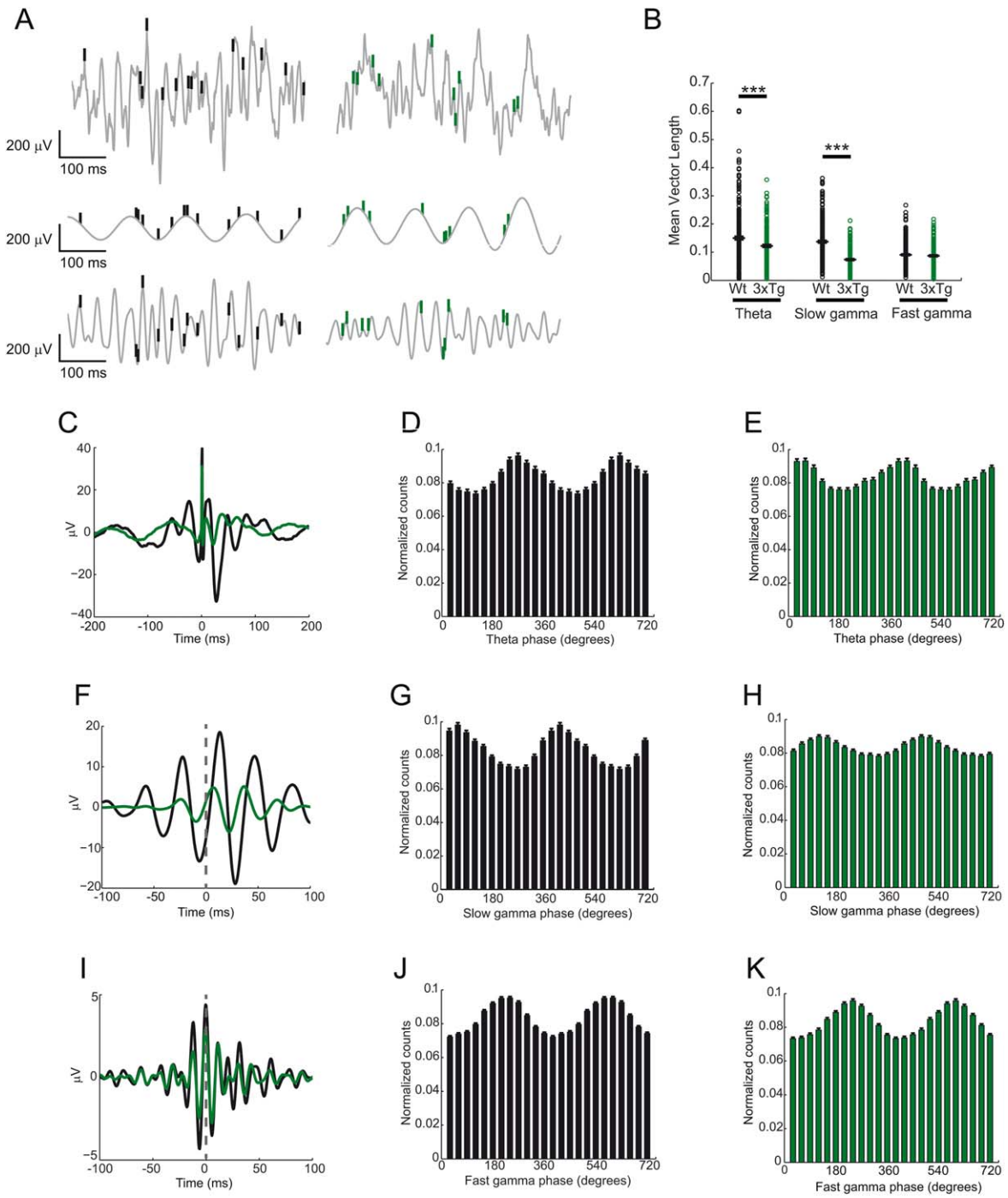

FIGURE 4. Rhythmic coordination of place cells by theta and slow gamma oscillations was abnormal in 3xTg mice. (A) Example LFP recordings, with spikes from 3xTg (green, right) and Wt (black, left) mice. Unfiltered LFP traces (top), theta (6–10 Hz) filtered LFP traces (middle), and slow gamma (25–55 Hz) filtered LFP traces (bottom) are shown in grey. The strength of phase-locking to theta and slow gamma rhythms was significantly lower in 3xTg mice. (B) Mean vector lengths of spike-phase distributions for theta and slow gamma were significantly lower for 3xTg place cells than for Wt place cells. Circles indicate mean vector lengths for individual place cells. (C) Spike time averages (STA) of unfiltered LFP traces for Wt (black) and 3xTg (green) mice. (D,E) Spike time-theta phase distributions for (D) Wt and (E) 3xTg mice. Note a shift in the preferred theta phase of place cell spiking in 3xTg mice. (F) Same as C but for slow gamma-filtered LFP. (G,H) Slow gamma phase distributions for place cell spike times from (G) Wt and (H) 3xTg mice. Note a shift in the preferred spiking phase of slow gamma for place cells recorded from 3xTg mice and a decreased preference to fire at this phase. (I–K) Same as F–H but for fast gamma. Note that phase-locking of 3xTg and Wt place cell spikes to fast gamma was comparable. (F and I) The grey dashed line signifies time of spike occurrence.

TABLE 1.

Number of Cells Recorded and Number of Circular Track Laps Run by Each Mouse on Each Recording Day

Mouse	Recording day	Number of cells	Number of laps (session: 1, 2, 3)
3xTg 1	1	12	17, 15, 16
	2	13	18, 17, 24
	3	7	15, 15, 15
	4	18	13, 14, 16
	5	9	17, 20, 23
	6	20	14, 16, 18
	7	18	15, 24, 28
	8	19	15, 16, 18
3xTg 2	1	7	20, 16, 16
	2	14	25, 23, 13
	3	14	14, 14, 17
	4	11	18, 16, 13
	5	7	19, 20, 20
	6	3	16, 16, 16
	7	2	19, 22, 23
3xTg 3	1	1	11, 11, 14
	2	3	13, 13, 13
	3	2	11, 11, 12
	4	3	15, 18, 15
	5	3	14, 12, 13
	6	3	9, 14, 14
	7	4	11, 11, 11
	8	2	11, 14, 18
	9	3	20, 21, 16
Wt 1	1	13	11, 11, 12
	2	16	11, 12, 14
	3	8	13, 10, 13
	4	13	14, 11, 12
	5	25	10, 12, 14
	6	22	11, 11, 12
	7	22	13, 13, 13
Wt 2	1	2	18, 17, 11
	2	1	14, 13, 12
	No CA1 cells recorded on this day		
	4	2	21, 15, 22
	5	4	17, 17, 20
	6	5	17, 16, 16
	7	10	16, 27, 21
	8	9	18, 16, 18
	9	12	26, 26, 23
	10	13	27, 26, 19
Wt 3	1	3	13, 14, 15
	2	8	17, 16, 19
	3	9	17, 14, 15
	4	12	19, 18, 21
	5	13	14, 14, 18
	6	16	25, 25, 27
	7	17	17, 23, 22

power in 2-Hz-wide frequency bands from 2 to 100 Hz was estimated for individual theta cycles, using the wavelet transform method described above. Time-frequency representations of power for multiple theta cycles recorded from the same tetrode and session within the same animal were then averaged. Power estimates from the first behavioral session of each recording day for each tetrode with place cells were then averaged and *z*-scored. *z*-scored power estimates were then averaged across recording days for each mouse. The grand average time frequency representations of power shown in Figure 5 were created by then averaging across all mice within each genotype.

Histology

For verification of tetrode locations, brains were cut coronally (1 mouse) or sagittally (5 mice) at 30 μm and stained with cresyl violet. Each section through the relevant part of the hippocampus was collected. All tetrode locations were identified, and the tip of each tetrode was localized by comparison across adjacent sections.

Immunohistochemistry

Sections that had been mounted for histological verification had coverslips removed by xylene. Sections were then rehydrated through a graded series of ethanol/water solutions (100%, 90%, 80%, 70%, and 50%) for 4 min each, followed by a final incubation in distilled water (4 min). Sections from naïve 11- to 12-month-old mice were added for the water incubation; from this point on, slides from tested mice and naïve mice were treated the same. Endogenous peroxidase activity was quenched by incubation in 0.3% hydrogen peroxide in methanol, for 10 min at room temperature (RT). Sections were boiled in Citrate buffer (BioGenex, San Ramon, CA) for 5 min and incubated in 88% formic acid for 10 min, prior to blocking with 10% goat serum in Tris-buffered saline (TBS), pH 7.4, for 20 min at RT. Sections were incubated overnight at 4°C with pan-Aβ polyclonal antibody, DW6 (1:1000 dilution). Sections were washed with TBS and incubated with biotinylated goat anti-rabbit secondary antibody (Vector Laboratories Inc., Burlingame, CA), diluted in 10% goat serum at RT. Thereafter, sections were incubated with horseradish-peroxidase (from a Vector Elite ABC kit, Vector Laboratories Inc.) for 30 min at RT. Diaminobenzidine (DAB; Sigma Chemical Co., St. Louis, MO) was then added to sections and incubated until sufficient color development was obtained on the positive control sections. DAB development was stopped by incubation in water. Sections were dehydrated through graded ethanol/water solutions (50%, 70%, 80%, 90%, and 100%), cleared by incubation in xylene, and coverslipped under Eukitt mounting medium (Electron Microscopy Sciences, Hatfield, PA).

RESULTS

To determine whether place cell firing properties and rhythmic coordination were altered in the 3xTg model of AD, we collected spikes from single units together with continuously

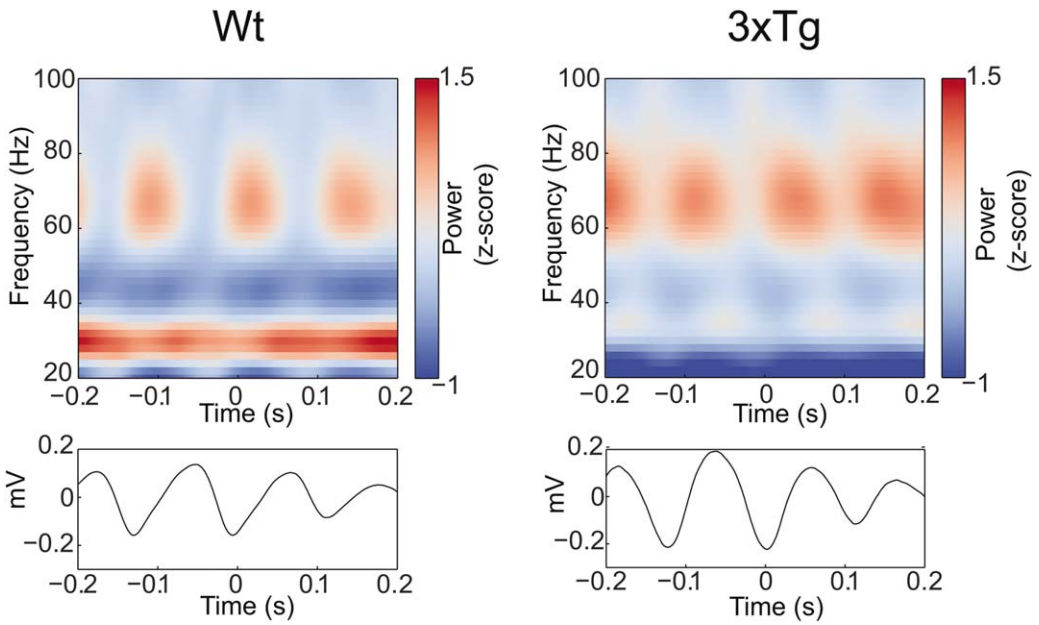

FIGURE 5. Theta-modulated slow gamma power in Wt and 3xTg mice. Time frequency representations of power for Wt (top left panel) and 3xTg (top right panel) mice. Power was *z*-scored and color-coded. In these figures, a prewhitening filter was applied for illustration purposes. Gamma power was aligned according to the trough of co-occurring theta rhythms (bottom panels show average of all detected theta cycles; time = 0 corresponds to the detected theta troughs). Note that the slow gamma band (25–40 Hz) that is apparent in Wt mice is diminished in 3xTg mice. Data shown are from the first session of each recording day for all mice of corresponding genotype.

sampled LFPs in stratum pyramidale of hippocampal subfield CA1 in 8–9-month-old 3xTg and Wt mice. The day after final recordings were completed, mice were sacrificed, allowing us to test for the occurrence of AD-like pathology around the time when the recordings were collected. To test for the presence of Aβ pathology, we stained tissue sections with the polyclonal anti-Aβ antibody, DW6. Although intraneuronal Aβ has been detected in 3xTg mice as early as 4 months old (Oddo et al., 2003b), we did not detect intraneuronal or extracellular amyloid deposits in our 8–9-month-old 3xTg mice, using DW6 antibody (Fig. 1C,D). To confirm that these mice develop AD-related pathology at older ages, we used DW6 antibody to assess the extent of amyloid pathology in 11–12-month-old naïve 3xTg mice. We detected intraneuronal deposits in the neocortex and hippocampus of 3xTg mice at this age that were not apparent in age-matched Wt mice (Fig. 1E,F). Aβ pathology is thought to precede and give rise to tau pathology in 3xTg mice (Oddo et al., 2003a, 2006). No Aβ deposition was observed in the brains of 3xTg mice at the ages when recordings were collected, and thus tau pathology was not assessed. However, enlarged ventricles were apparent in all of the 3xTg mouse brains at 8–9 and 11–12 months old but were not observed in any of the age-matched Wt mouse brains (Fig. 1C,F).

To assess whether place cell firing patterns were disrupted in 3xTg mice, we recorded 198 place cells (with a total of 274 place fields) in three 3xTg mice and 255 place cells (with a total of 364 place fields) in three Wt mice. Recordings took place across 7–10 consecutive days while mice traversed a familiar circular track. The number of laps completed each day was similar in Wt and 3xTg mice (Mann–Whitney U; $Z = -0.1$, $P = 0.9$, Table 1). Recording across three 10-min sessions each day enabled us to compare the stability of place cell maps across successive sessions within each day to determine whether place map stability was impaired in 3xTg mice as in other AD models (Cheng and Ji, 2013; Zhao et al., 2014; Booth et al., 2016). Example rate maps from representative place cells are shown for Wt and 3xTg mice (Fig. 2). As is apparent in these examples, 3xTg place cell rate maps appeared less stable across sessions than Wt rate maps. Instabilities in place cell maps may involve shifts in place field locations, changes in place cell firing rates, or both. To determine the extent to which place field locations shifted across time in 3xTg mice, we calculated spatial correlations between all pairs of sessions within each day. Due to the increased time between sessions 1 and 3, it was expected that the spatial correlation for this session pair would be lower than corresponding spatial correlations for the other session pairs (i.e., 1–2 and 2–3). Accordingly, a significant effect of time interval on spatial correlations was observed (mixed ANOVA; main effect of session pair: $F(1.9, 852.2) = 42.7$, $P < 0.0001$; Fig. 3A). More interestingly though, overall spatial correlations were lower for 3xTg mice than Wt mice (mixed ANOVA; main effect of genotype: $F(1, 451) = 4550.4$, $P < 0.0001$; Fig. 3A), suggesting that place field locations were less stable across sessions in 3xTg mice compared to controls. To examine whether place cell firing

rates were also less stable across sessions in 3xTg mice, we assessed whether mean firing rates changed significantly across sessions using a "rate overlap" measure (see Materials and Methods). We found that the overlap in firing rates between session pairs for 3xTg place cells was significantly diminished compared to Wt place cells (mixed ANOVA; main effect of genotype: $F(1,451) = 7855.4$, $P < 0.0001$; Fig. 3B), indicating that place cell firing rates were less stable across time in 3xTg mice than in Wt mice. As expected, there was again a main effect of session pair (mixed ANOVA; $F(1.9, 853.8) = 21.2$, $P < 0.0001$; Fig. 3B), indicating that firing rates differed most between the 2 sessions that were furthest apart in time. We also assessed spatial correlation and rate overlap measures in individual animals for each genotype to ensure that the observed deficits in place cell stability were consistent across 3xTg mice. There were no significant differences in spatial correlation or rate overlap measures across individual mice within each genotype (spatial information, mixed ANOVA; main effect of Wt subject: $F(2,252) = 2.7$, $P = 0.07$; main effect of 3xTg subject: $F(2,195) = 0.8$, $P = 0.5$; rate overlap, mixed ANOVA; main effect of Wt subject: $F(2,252) = 0.7$, $P = 0.5$; main effect of 3xTg subject: $F(2,195) = 0.8$, $P = 0.5$). Moreover, spatial correlation and rate overlap scores were typically higher for individual Wt mice compared to individual 3xTg mice (Supporting Information, Figs. S1A,B).

In addition to assessing place cell stability across sessions, we also compared lap-to-lap stability of place cell firing within each session. Spike raster plots for example 3xTg and Wt place cells are shown (Figs. 3C,D). As is apparent in these examples, place cell firing was less stable across laps in 3xTg mice than in Wt mice. These observations were supported by significantly lower lap-by-lap spatial correlation measures (Mann–Whitney U; $Z = -9.3$, $P < 0.0001$; Fig. 3E) and rate overlap scores (Mann–Whitney U; $Z = -7.0$, $P < 0.0001$; Fig. 3F) in 3xTg mice compared to Wt mice. These results demonstrate that, although place cells from 3xTg mice exhibited well defined place fields, the place fields were relatively unstable across repeated exposures to the same familiar locations.

Besides stability across time, other deficits in 3xTg place fields were also evident, consistent with results from other AD models (Cacucci et al., 2008; Cheng and Ji, 2013; Witton et al., 2014; Zhao et al., 2014; Cayzac et al., 2015; Booth et al., 2016). Spatial information was significantly lower for place cells in 3xTg mice compared to those in Wt mice (Mann–Whitney U; $Z = -2.2$, $P = 0.03$; Fig. 3G). Furthermore, 3xTg place cells had significantly diminished mean firing rates (Wt: 0.6 ± 0.03 Hz, 3xTg: 0.5 ± 0.03 Hz; Mann–Whitney U; $Z = -3.7$, $P < 0.0001$; Fig. 3H), peak in-field firing rates (calculated as the peak in-field firing rate across the 3 sessions; Wt: 7.8 ± 0.2 Hz, 3xTg: 6.0 ± 0.2 Hz, Mann–Whitney U; $Z = -4.23$, $P < 0.0001$; Fig. 3I), and mean in-field firing rates (Wt: 3.8 ± 0.1 Hz, 3xTg: 2.8 ± 0.1 Hz, Mann–Whitney U; $Z = -5.2$, $P < 0.0001$; Fig. 3J). On the other hand, place field size and number of place fields per cell were consistent across Wt and 3xTg mice (Supporting Information, Table S1).

In addition to differences in place field firing properties, we also observed that 3xTg mice had significantly lower daily mean running speeds than Wt mice (Wt: 8.1 ± 0.4 cm/s, 3xTg: 6.4 ± 0.4 cm/s; Mann–Whitney U; $Z = -2.7$, $P = 0.008$; Supporting Information, Table S1). Running speed has previously been shown to affect firing rates of place cells in rats (McNaughton et al., 1983; Wiener et al., 1989; Geisler et al., 2007; Zheng et al., 2015). To assess whether firing rate changes were due to differences in running speed between Wt and 3xTg mice, we removed place cells recorded on the fastest and slowest days for Wt and 3xTg mice, respectively. The average running speeds of Wt and 3xTg mice on the remaining recording days were highly comparable (Wt: 7.3 ± 0.2 cm/s, 3xTg: 7.1 ± 0.4 cm/s; Mann–Whitney U; $Z = -0.7$, $P = 0.5$; Supporting Information, Table S1). We then examined place cell firing properties for this subset of place cells recorded during roughly equivalent running speeds (204 place cells, with 298 place fields, from three Wt mice; 181 place cells, with 253 place fields, from three 3xTg mice). In this reduced data set, place cells from 3xTg mice continued to show decreased spatial correlations between sessions (mixed ANOVA; main effect of genotype: $F(1, 383) = 15.8$, $P < 0.0001$) and reduced overlap in firing rates between sessions (mixed ANOVA; main effect of genotype: $F(1, 383) = 10.5$, $P < 0.001$), compared to place cells from Wt mice. Additionally, as expected and as was observed in the full data set, spatial correlations and rate overlap measures were affected by time between compared sessions (main effect of session pair on spatial correlations: $F(1.9, 723.6) = 35.8$, $P < 0.0001$; main effect of session pair on rate overlap: $F(1.9, 727.1) = 18.1$, $P < 0.0001$). Furthermore, lap-by-lap place cell stability remained significantly impaired in 3xTg mice (spatial correlation, Mann–Whitney U; $Z = -8.9$, $P < 0.0001$; rate overlap, Mann–Whitney U; $Z = -7.2$, $P < 0.0001$). In this reduced data set, 3xTg place cells continued to have lower firing rates than Wt place cells (mean firing rate, Mann–Whitney U; $Z = -2.8$, $P = 0.006$; peak in-field firing rate, $Z = -3.2$, $P = 0.001$; mean in-field firing rate, $Z = -4.1$, $P < 0.0001$), but there was no longer a significant decrease in the amount of spatial information conveyed by 3xTg place cells (Mann–Whitney U; $Z = -1.3$, $P = 0.2$). Taken together, these results suggest that aberrant place cell firing properties observed in 3xTg mice were not merely a result of differences in animals' running speeds.

Place cell firing is modulated by theta and gamma rhythms (Bieri et al., 2014; Csicsvari et al., 2003; O'Keefe and Recce, 1993; Skaggs et al., 1996; Zheng et al., 2016). Much evidence supports the conclusion that theta rhythms are important for memory operations (Colgin, 2013). Moreover, fast and slow gamma rhythms have been hypothesized to promote memory encoding and retrieval, respectively (Bieri et al., 2014; Colgin, 2016; Colgin and Moser, 2010). Therefore, it is conceivable that spatial memory impairments reported in 3xTg mice (Billings et al., 2005) arise in part due to deficient temporal organization of place cell spikes by theta and gamma rhythms. Yet, to our knowledge, rhythmic modulation of place cell spiking by fast and slow gamma rhythms has not previously been

assessed in a mouse model of AD. We thus assessed the extent to which place cell spikes phase-locked to gamma and theta rhythms in 3xTg mice compared to Wt mice (Fig. 4 and Supporting Information, Fig. S2). The proportions of place cells that were significantly phase-locked to theta rhythms and slow gamma rhythms were significantly lower for 3xTg mice than Wt mice (85.9% of Wt cells phase-locked to theta vs. 77.8% of 3xTg cells phase-locked to theta, binomial test, $P = 0.004$; 84.3% of Wt cells phase-locked to slow gamma vs. 48.9% of 3xTg cells phase-locked to slow gamma, binomial test, $P < 0.0001$). Analogous effects were not observed for fast gamma modulation of spiking (68.2% of Wt cells and 65.2% of 3xTg cells phase-locked to fast gamma, binomial test, $P = 0.2$). Moreover, we assessed the strength of place cell spike phase-locking for all cells and identified a significant interaction effect of genotype and brain rhythm type (mixed ANOVA; genotype $\times$ rhythm type interaction effect: $F(1.6, 731.9) = 20.8$, $P < 0.0001$; Fig. 4B). Post hoc testing showed that place cell spikes were more weakly phase-locked to theta ($F(1,451) = 11.5$, $P = 0.001$) and slow gamma rhythms ($F(1,451) = 113.1$), $P < 0.0001$), but not fast gamma rhythms ($F(1,451) = 0.6$, $P = 0.4$), in 3xTg mice compared to Wt mice. We also assessed the strength of phase-locking of place cells in each of the individual mice. Theta and slow gamma phase-locking of spikes within individual mice was generally stronger for Wt mice compared to 3xTg mice (Supporting Information, Fig. S1C). However, fast gamma phase-locking was similar in individual Wt and 3xTg mice.

Furthermore, the preferred theta and slow gamma phases at which place cell spikes tended to occur differed for Wt and 3xTg mice. Spike-triggered averages of slow gamma activity and slow gamma phase distributions for spike times revealed that 3xTg cells preferentially fired on a later phase of the slow gamma cycle than Wt place cells (Watson–Williams test: $F(1,451) = 38.7$, $P < 0.0001$; Figs. 4F–H). A significant shift in the preferred phase of place cell spiking was also observed for theta (Watson–Williams test: $F(1,451) = 155.4$, $P < 0.0001$; Figs. 4C–E). In contrast, no shift in the preferred fast gamma phase of spikes was detected (Watson–Williams test: $F(1,451) = 3.3$, $P = 0.07$; Figs. 4I–K).

The above-described pattern of results did not change when rhythmic modulation of place cell firing was assessed in the subset of data in which running speeds were comparable across genotypes (86.8% of cells phase-locked to theta in Wt mice vs. 79.6% of cells phase-locked to theta in 3xTg mice, binomial test, $P = 0.005$; 85.3% of cells phase-locked to slow gamma in Wt mice vs. 48.6% of cells phase-locked to slow gamma in 3xTg mice, binomial test, $P < 0.0001$; genotype $\times$ rhythm type interaction effect on mean vector lengths, mixed ANOVA, $F(1.6, 619.4) = 25.2$, $P < 0.0001$; post hoc tests: theta: $F(1,383) = 7.7$, $P = 0.006$; slow gamma: $F(1,383) = 119.9$, $P < 0.0001$). Preferred spike time phases for theta and slow gamma also remained significantly altered for 3xTg place cells in the reduced data set (Watson–Williams test; theta phase: $F(1,383) = 155.5$, $P < 0.0001$; slow gamma phase: $F(1,383) = 37.3$, $P < 0.0001$).

To ascertain whether the observed reduction in phase-locking to slow gamma was accompanied by a reduction in slow gamma power, we estimated gamma power across theta cycles in Wt and 3xTg mice (Fig. 5). Slow and fast gamma power were maximal at particular theta phases, as expected based on coupling between theta phase and slow and fast gamma power in normal healthy rats (Colgin et al., 2009). However, theta phase-coupled increases in slow gamma power were less apparent in 3xTg mice compared to Wt mice, whereas phasic increases in fast gamma power remained robust in 3xTg mice. Given the apparent reduction in slow gamma power (Fig. 5) and significant impairment in slow gamma phase-locking of spikes in 3xTg mice (Fig. 4B), we investigated the extent to which slow gamma power predicted slow gamma phase-locking strength. A multiple regression analysis was performed to predict mean vector lengths of slow gamma phase distributions for place cell spikes based on genotype, slow gamma power, and the genotype $\times$ slow gamma power interaction. Overall, this group of variables significantly predicted the strength of slow gamma phase-locking of place cell spikes (multiple regression model: $F(3,449) = 39.1$, $P < 0.0001$). Moreover, the effects of genotype and the genotype $\times$ slow gamma power interaction were significant (multiple regression model; genotype, $b = -0.06$, $t(449) = -9.0$, $P < 0.0001$; genotype $\times$ slow gamma power interaction, $b = 0.03$, $t(449) = 2.0$, $P = 0.05$). When we assessed the extent to which slow gamma power predicted phase-locking strength separately for 3xTg and Wt place cells, we found that slow gamma power significantly predicted mean vector length values in 3xTg but not WT mice (3xTg: $b = 0.02$, $t(196) = 2.2$, $P = 0.03$; Wt: $b = -0.01$, $t(253) = -1.1$, $P = 0.3$). Together with the impairments in slow gamma rhythmic modulation of spikes reported above, the results presented here suggest that slow gamma modulation of hippocampal activity is impaired in the 3xTg model of AD.

DISCUSSION

Here, we examined place cell representations of space and rhythmic coordination of place cells in the 3xTg mouse model of AD. These mice showed impairments in the stability of place cell maps and reductions in place cell firing rates that were consistent with a number of other rodent models of AD that overexpress disease-related tau and/or APP mutations (Cheng and Ji, 2013; Witton et al., 2014; Zhao et al., 2014; Ciupek et al., 2015; Booth et al., 2016). We also found that rhythmic coordination of place cell spiking by theta and slow gamma rhythms, but not fast gamma rhythms, was disrupted in freely behaving 3xTg mice. Such a dissociation between slow and fast gamma impairments in an AD model may help explain why some AD studies have reported gamma rhythm deficits while others have not (Herrmann and Demiralp, 2005).

With regard to place cell abnormalities in 3xTg mice, analysis of place cell activity revealed that place fields were less stable across the three daily sessions, and also across laps within each session, in 3xTg mice compared to Wt mice (Figs. 2 and 3). Decreased stability was observed for both place field locations and firing rates. These results are consistent with prior studies that tested place field stability over consecutive laps (Cheng and Ji, 2013; Ciupek et al., 2015; Booth et al., 2016) or sessions (Zhao et al., 2014) in other AD mouse models. In the latter study, the authors also used a Morris water maze (MWM) task to assess spatial memory at the behavioral level and found that $APP_{Swe/Ind}$ mice were deficient in spatial memory recall. These findings suggest that unstable spatial memory representations in place cells may contribute to impairments in spatial memory retrieval.

Interestingly, slow gamma has previously been proposed to promote memory retrieval (Colgin, 2015). This proposal was based in part on results showing that CA3 and CA1 are coupled by slow gamma in familiar environments (Colgin et al., 2009) and that CA3–CA1 connectivity is required for retrieval of spatial representations and memories (Brun et al., 2002; Steffenach et al., 2002; Nakashiba et al., 2008). If slow gamma promotes retrieval of stored spatial memory representations from CA3 to CA1, then the abnormal slow gamma coordination of place cells that we observed in 3xTg mice (Fig. 4) may prevent proper retrieval of stored memories. Failure to correctly retrieve previously stored spatial memory representations from CA3 would perhaps result in CA1 place cells having to construct a representation of spatial location using only inconstant sensory cues and path integration, which accumulates error over time. This raises the possibility that increased instability of CA1 place cell maps in 3xTg mice arises in part due to impaired slow gamma coordination of place cells.

Although we did not test for behavioral impairments in spatial memory in 3xTg mice in this study, these mice have previously been shown to exhibit memory deficits at the age that we tested and at younger ages (Billings et al., 2005; Gimenez-Llort et al., 2007; Sterniczuk et al., 2010). Specifically, when tested on consecutive days in the MWM, 3xTg mice performed significantly worse on the first trial of a new day than the last trial of a previous day (Billings et al., 2005). This behavioral deficit is consistent with a failure to retrieve memories that were stored on a previous day. Moreover, a recent study reported memory retrieval deficits in several mouse models of AD, including 3xTg mice (Roy et al., 2016). It is possible that 3xTg mice in these prior studies exhibited place cell firing and rhythmic coordination deficits similar to those observed in this study and those deficits contributed to the reported memory retrieval impairments.

This study focused on place cell representations and hippocampal rhythms during active behaviors. However, memory retrieval may also involve replay of previous experiences by hippocampal place cells during sharp wave-ripples (SWRs) in inactive behaviors (Carr et al., 2011; Pfeiffer and Foster, 2013). Furthermore, slow gamma coupling of CA3 and CA1 during SWRs may facilitate such retrieval (Carr et al., 2012). Results from a recent study of SWRs in AD mice found that deficiencies in SWR-associated slow gamma may produce memory retrieval impairments in AD. Specifically, in mice expressing the AD risk factor apolipoprotein E4, slow gamma during SWRs was abnormally low (Gillespie et al., 2016). Remarkably, pharmacogenetic manipulations that restored SWR-associated slow gamma in these mice also alleviated memory impairments (Knoferle et al., 2014; Gillespie et al., 2016). Moreover, a subsequent study reported that slow gamma rhythms were diminished during SWRs in the 5xTg mouse model of AD and that inducing slow gamma rhythms in these mice reduced Aβ levels (Iaccarino et al., 2016). Taken together with the results discussed above, these findings support the conclusion that disrupted slow gamma contributes to behavioral and neuronal abnormalities in AD during both active and inactive behavioral states.

In addition to the slow gamma disturbances discussed above, we also observed aberrations in theta rhythmic modulation of place cell activity. These results are in line with previous studies that reported abnormal theta rhythms in both tau and APP transgenic mouse models of AD (Villette et al., 2010; Cantero et al., 2011; Scott et al., 2012; Cheng and Ji, 2013; Schneider et al., 2014; Cayzac et al., 2015; Ciupek et al., 2015; Booth et al., 2016). Moreover, a study that utilized the APP/PS1 mouse model demonstrated a shift in the preferred theta phase of putative pyramidal cell spikes in transgenic mice (Cayzac et al., 2015), consistent with the shift in theta phases of place cell spikes in AD mice in this study. The authors of the earlier study speculated that the observed shift could be due to running speed differences. However, we observed abnormalities in theta modulation of place cell spiking that persisted in a subset of data in which running speeds were approximately equivalent across genotypes. Considering that theta rhythms are thought to organize sequences of place cells during retrieval of spatial memories (Lisman and Redish, 2009), disturbances in theta coordination of place cell spiking could contribute to the memory retrieval deficits in AD mice discussed above. Interestingly, place cell spikes are thought to occur on different phases of theta depending on whether the brain is encoding or retrieving information (Hasselmo et al., 2002; Manns et al., 2007). Our observation that place cell spikes in 3xTg mice occur closer to the trough of theta may thus suggest that the hippocampal network in 3xTg mice is biased against retrieving previously stored memories. However, this possibility requires further investigation.

Our current data, taken together with earlier results, raise the possibility that disturbed slow gamma and theta rhythmic organization of place cell activity contributes to unstable spatial memories, and corresponding impairments in behaviors requiring spatial memory processing, in AD. However, one caveat to keep in mind is that overexpression of APP has been linked to EEG abnormalities in young mice, independent of AD-related pathology (Born et al., 2014). Therefore, much work still remains to be done to determine whether effects similar to those reported here contribute to memory impairments in AD. With further investigation, a better understanding of aberrant

brain rhythms in AD could aid in earlier diagnosis of AD or provide a novel therapeutic strategy aimed at restoring healthy rhythmic activity.

Acknowledgments

The authors thank Katelyn N. Bobbitt and Kayli Kallina for technical assistance, Nicole Alexander for help with animal training, and Chenguang Zheng for kindly providing Matlab code for some of the analyses. The authors also thank Dominic M. Walsh (Brigham & Women's Hospital and Harvard Medical School, Boston) for kindly providing DW6 antibody and Boris V. Zemelman for generously providing animals for this project and for helpful discussions. The authors acknowledge the Texas Advanced Computing Center (TACC) at The University of Texas at Austin for providing data storage resources that have contributed to the research described within this article. URL: http://www.tacc.utexas.edu. The authors declare no competing financial interests.

REFERENCES

Albert MS. 2011. Changes in cognition. Neurobiol Aging 32 Suppl 1: S58–S63.

Bieri KW, Bobbitt KN, Colgin LL. 2014. Slow and fast gamma rhythms coordinate different spatial coding modes in hippocampal place cells. Neuron 82:670–681.

Billings LM, Oddo S, Green KN, McGaugh JL, LaFerla FM. 2005. Intraneuronal Abeta causes the onset of early Alzheimer's disease-related cognitive deficits in transgenic mice. Neuron 45:675–688.

Booth CA, Witton J, Nowacki J, Tsaneva-Atanasova K, Jones MW, Randall AD, Brown JT. 2016. Altered intrinsic pyramidal neuron properties and pathway-specific synaptic dysfunction underlie aberrant hippocampal network function in a mouse model of tauopathy. J Neurosci 36:350–363.

Born HA, Kim JY, Savjani RR, Das P, Dabaghian YA, Guo Q, Yoo JW, Schuler DR, Cirrito JR, Zheng H, Golde TE, Noebels JL, Jankowsky JL. 2014. Genetic suppression of transgenic APP rescues hypersynchronous network activity in a mouse model of Alzeimer's disease. J Neurosci 34:3826–3840.

Brun VH, Otnass MK, Molden S, Steffenach HA, Witter MP, Moser MB, Moser EI. 2002. Place cells and place recognition maintained by direct entorhinal-hippocampal circuitry. Science 296:2243–2246.

Cacucci F, Yi M, Wills TJ, Chapman P, O'Keefe J. 2008. Place cell firing correlates with memory deficits and amyloid plaque burden in Tg2576 Alzheimer mouse model. Proc Natl Acad Sci USA 105: 7863–7868.

Cantero JL, Moreno-Lopez B, Portillo F, Rubio A, Hita-Yanez E, Avila J. 2011. Role of tau protein on neocortical and hippocampal oscillatory patterns. Hippocampus 21:827–834.

Carr MF, Jadhav SP, Frank LM. 2011. Hippocampal replay in the awake state: A potential substrate for memory consolidation and retrieval. Nat Neurosci 14:147–153.

Carr MF, Karlsson MP, Frank LM. 2012. Transient slow gamma synchrony underlies hippocampal memory replay. Neuron 75:700–713.

Cayzac S, Mons N, Ginguay A, Allinquant B, Jeantet Y, Cho YH. 2015. Altered hippocampal information coding and network synchrony in APP-PS1 mice. Neurobiol Aging 36:3200–3213.

Cheng J, Ji D. 2013. Rigid firing sequences undermine spatial memory codes in a neurodegenerative mouse model. eLife 2:e00647.

Ciupek SM, Cheng J, Ali YO, Lu HC, Ji D. 2015. Progressive functional impairments of hippocampal neurons in a tauopathy mouse model. J Neurosci 35:8118–8131.

Colgin LL. 2013. Mechanisms and functions of theta rhythms. Ann Rev Neurosci 36:295–312.

Colgin LL. 2015. Do slow and fast gamma rhythms correspond to distinct functional states in the hippocampal network? Brain Res 1621:309–315.

Colgin LL. 2016. Rhythms of the hippocampal network. Nat Rev Neurosci 17:239–249.

Colgin LL, Denninger T, Fyhn M, Hafting T, Bonnevie T, Jensen O, Moser MB, Moser EI. 2009. Frequency of gamma oscillations routes flow of information in the hippocampus. Nature 462:353–357.

Colgin LL, Leutgeb S, Jezek K, Leutgeb JK, Moser EI, McNaughton BL, Moser MB. 2010. Attractor-map versus autoassociation based attractor dynamics in the hippocampal network. J Neurophysiol 104:35–50.

Colgin LL, Moser EI. 2010. Gamma oscillations in the hippocampus. Physiology (Bethesda) 25:319–329.

Csicsvari J, Jamieson B, Wise KD, Buzsaki G. 2003. Mechanisms of gamma oscillations in the hippocampus of the behaving rat. Neuron 37:311–322.

Ferri CP, Prince M, Brayne C, Brodaty H, Fratiglioni L, Ganguli M, Hall K, Hasegawa K, Hendrie H, Huang Y, Jorm A, Mathers C, Menezes PR, Rimmer E, Scazufca M. 2005. Global prevalence of dementia: A Delphi consensus study. Lancet 366:2112–2117.

Fox SE, Ranck JB. Jr. 1981. Electrophysiological characteristics of hippocampal complex-spike cells and theta cells. Exp Brain Res 41: 399–410.

Geisler C, Robbe D, Zugaro M, Sirota A, Buzsaki G. 2007. Hippocampal place cell assemblies are speed-controlled oscillators. Proc Natl Acad Sci USA 104:8149–8154.

Gillespie AK, Jones EA, Lin YH, Karlsson MP, Kay K, Yoon SY, Tong LM, Nova P, Carr JS, Frank LM, Huang Y. 2016. Apolipoprotein E4 causes age-dependent disruption of slow gamma oscillations during hippocampal sharp-wave ripples. Neuron 90:740–751.

Gimenez-Llort L, Blazquez G, Canete T, Johansson B, Oddo S, Tobena A, LaFerla FM, Fernandez-Teruel A. 2007. Modeling behavioral and neuronal symptoms of Alzheimer's disease in mice: A role for intraneuronal amyloid. Neurosci Biobehav Rev 31:125–147.

Girden ER. 1992. ANOVA: Repeated Measures: Newbury Park, CA: Sage.

Harris KD, Henze DA, Csicsvari J, Hirase H, Buzsaki G. 2000. Accuracy of tetrode spike separation as determined by simultaneous intracellular and extracellular measurements. J Neurophysiol 84: 401–414.

Hasselmo ME, Bodelon C, Wyble BP. 2002. A proposed function for hippocampal theta rhythm: Separate phases of encoding and retrieval enhance reversal of prior learning. Neural Comput 14: 793–817.

Henze DA, Borhegyi Z, Csicsvari J, Mamiya A, Harris KD, Buzsaki G. 2000. Intracellular features predicted by extracellular recordings in the hippocampus in vivo. J Neurophysiol 84:390–400.

Herrmann CS, Demiralp T. 2005. Human EEG gamma oscillations in neuropsychiatric disorders. Clin Neurophysiol 116:2719–2733.

Hodges JR. 2000. Memory in the dementias. In: Tulving E and Craik FIM, editors. The Oxford Handbook of Memory. New York: Oxford University Press.

Hollup SA, Molden S, Donnett JG, Moser MB, Moser EI. 2001. Accumulation of hippocampal place fields at the goal location in an annular watermaze task. J Neurosci 21:1635–1644.

Huynh H, Feldt LS. 1976. Estimation of the box correction for degrees of freedom from samples data in randomized block and split-plot designs. J Educ Stat 1:69–82.

Iaccarino HF, Singer AC, Martorell AJ, Rudenko A, Gao F, Gillingham TZ, Mathys H, Seo J, Kritskiy O, Abdurrob F, Adaikkan C, Canter RG, Rueda R, Brown EN, Boyden ES, Tsai LH. 2016. Gamma frequency entrainment attenuates amyloid load and modifies microglia. Nature 540:230–235.

Ittner AA, Gladbach A, Bertz J, Suh LS, Ittner LM. 2014. p38 MAP kinase-mediated NMDA receptor-dependent suppression of hippocampal hypersynchronicity in a mouse model of Alzheimer's disease. Acta Neuropathol Commun 2:149.

Knoferle J, Yoon SY, Walker D, Leung L, Gillespie AK, Tong LM, Bien-Ly N, Huang Y. 2014. Apolipoprotein E4 produced in GABAergic interneurons causes learning and memory deficits in mice. J Neurosci 34:14069–14978.

Leutgeb JK, Leutgeb S, Treves A, Meyer R, Barnes CA, McNaughton BL, Moser MB, Moser EI. 2005. Progressive transformation of hippocampal neuronal representations in "morphed" environments. Neuron 48:345–358.

Lisman J, Redish AD. 2009. Prediction, sequences and the hippocampus. Philos Trans R Soc Lond B Biol Sci 364:1193–1201.

Manns JR, Zilli EA, Ong KC, Hasselmo ME, Eichenbaum H. 2007. Hippocampal CA1 spiking during encoding and retrieval: Relation to theta phase. Neurobiol Learn Memory 87:9–20.

McKhann GM, Knopman DS, Chertkow H, Hyman BT, Jack CR, Jr., Kawas CH, Klunk WE, Koroshetz WJ, Manly JJ, Mayeux R, Mohs RC, Morris JC, Rossor MN, Scheltens P, Carrillo MC, Thies B, Weintraub S, Phelps CH. 2011. The diagnosis of dementia due to Alzheimer's disease: Recommendations from the National Institute on Aging-Alzheimer's Association workgroups on diagnostic guidelines for Alzheimer's disease. Alzheimers Dement 7:263–269.

McNaughton BL, Barnes CA, O'Keefe J. 1983. The contributions of position, direction, and velocity to single unit activity in the hippocampus of freely-moving rats. Exp Brain Res 52:41–49.

Nakashiba T, Young JZ, McHugh TJ, Buhl DL, Tonegawa S. 2008. Transgenic inhibition of synaptic transmission reveals role of CA3 output in hippocampal learning. Science 319:1260–1264.

Nakazawa K, Quirk MC, Chitwood RA, Watanabe M, Yeckel MF, Sun LD, Kato A, Carr CA, Johnston D, Wilson MA, Tonegawa S. 2002. Requirement for hippocampal CA3 NMDA receptors in associative memory recall. Science 297:211–218.

O'Keefe J. 1976. Place units in the hippocampus of the freely moving rat. Exp Neurol 51:78–109.

O'Keefe J, Dostrovsky J. 1971. The hippocampus as a spatial map. Preliminary evidence from unit activity in the freely-moving rat. Brain Res 34:171–175.

O'Keefe J, Recce ML. 1993. Phase relationship between hippocampal place units and the EEG theta rhythm. Hippocampus 3:317–330.

Oddo S, Caccamo A, Kitazawa M, Tseng BP, LaFerla FM. 2003a. Amyloid deposition precedes tangle formation in a triple transgenic model of Alzheimer's disease. Neurobiol Aging 24:1063–1070.

Oddo S, Caccamo A, Shepherd JD, Murphy MP, Golde TE, Kayed R, Metherate R, Mattson MP, Akbari Y, LaFerla FM. 2003b. Triple-transgenic model of Alzheimer's disease with plaques and tangles: Intracellular Abeta and synaptic dysfunction. Neuron 39:409–421.

Oddo S, Caccamo A, Tran L, Lambert MP, Glabe CG, Klein WL, LaFerla FM. 2006. Temporal profile of amyloid-beta (Abeta) oligomerization in an in vivo model of Alzheimer disease. A link between Abeta and tau pathology. J Biol Chem 281:1599–1604.

Pfeiffer BE, Foster DJ. 2013. Hippocampal place-cell sequences depict future paths to remembered goals. Nature 497:74–79.

Roy DS, Arons A, Mitchell TI, Pignatelli M, Ryan TJ, Tonegawa S. 2016. Memory retrieval by activating engram cells in mouse models of early Alzheimer's disease. Nature 531:508–512.

Rubio SE, Vega-Flores G, Martinez A, Bosch C, Perez-Mediavilla A, del Rio J, Gruart A, Delgado-Garcia JM, Soriano E, Pascual M. 2012. Accelerated aging of the GABAergic septohippocampal pathway and decreased hippocampal rhythms in a mouse model of Alzheimer's disease. FASEB J 26:4458–4467.

Schneider F, Baldauf K, Wetzel W, Reymann KG. 2014. Behavioral and EEG changes in male 5xFAD mice. Physiol Behav 135:25–33.

Scott L, Feng J, Kiss T, Needle E, Atchison K, Kawabe TT, Milici AJ, Hajos-Korcsok E, Riddell D, Hajos M. 2012. Age-dependent disruption in hippocampal theta oscillation in amyloid-beta overproducing transgenic mice. Neurobiol Aging 33:1481 e13–1481 e23.

Skaggs WE, McNaughton BL, Wilson MA, Barnes CA. 1996. Theta phase precession in hippocampal neuronal populations and the compression of temporal sequences. Hippocampus 6:149–172.

Squire LR, Stark CE, Clark RE. 2004. The medial temporal lobe. Ann Rev Neurosci 27:279–306.

Steffenach HA, Sloviter RS, Moser EI, Moser MB. 2002. Impaired retention of spatial memory after transection of longitudinally oriented axons of hippocampal CA3 pyramidal cells. Proc Natl Acad Sci USA 99:3194–3198.

Sterniczuk R, Antle MC, Laferla FM, Dyck RH. 2010. Characterization of the 3xTg-AD mouse model of Alzheimer's disease: Part 2. Behavioral and cognitive changes. Brain Res 1348:149–155.

Tallon-Baudry C, Bertrand O, Delpuech C, Permier J. 1997. Oscillatory gamma-band (30-70 Hz) activity induced by a visual search task in humans. J Neurosci 17:722–734.

Treves A, Rolls ET. 1992. Computational constraints suggest the need for two distinct input systems to the hippocampal CA3 network. Hippocampus 2:189–199.

Villette V, Poindessous-Jazat F, Simon A, Lena C, Roullot E, Bellessort B, Epelbaum J, Dutar P, Stephan A. 2010. Decreased rhythmic GABAergic septal activity and memory-associated theta oscillations after hippocampal amyloid-beta pathology in the rat. J Neurosci 30:10991–11003.

Voigts J, Siegle JH, Pritchett DL, Moore CI. 2013. The flexDrive: An ultra-light implant for optical control and highly parallel chronic recording of neuronal ensembles in freely moving mice. Front Syst Neurosci 7:8.

Wiener SI, Paul CA, Eichenbaum H. 1989. Spatial and behavioral correlates of hippocampal neuronal activity. J Neurosci 9:2737–2763.

Witton J, Staniaszek LE, Bartsch U, Randall AD, Jones MW, Brown JT. 2014. Disrupted hippocampal sharp-wave ripple-associated spike dynamics in a transgenic mouse model of dementia. J Physiol.

Zhao R, Fowler SW, Chiang AC, Ji D, Jankowsky JL. 2014. Impairments in experience-dependent scaling and stability of hippocampal place fields limit spatial learning in a mouse model of Alzheimer's disease. Hippocampus 24:963–978.

Zheng C, Bieri KW, Hsiao YT, Colgin LL. 2016. Spatial sequence coding differs during slow and fast gamma rhythms in the hippocampus. Neuron 89:398–408.

Zheng C, Bieri KW, Trettel SG, Colgin LL. 2015. The relationship between gamma frequency and running speed differs for slow and fast gamma rhythms in freely behaving rats. Hippocampus 25: 924–938.